Science Advances

AAAS

Supplementary Materials for

Sequentially addressable dielectrophoretic array for high-throughput sorting of large-volume biological compartments

A. Isozaki*, Y. Nakagawa, M. H. Loo, Y. Shibata, N. Tanaka, D. L. Setyaningrum, J.-W. Park, Y. Shirasaki, H. Mikami, D. Huang, H. Tsoi, C. T. Riche, T. Ota, H. Miwa, Y. Kanda, T. Ito, K. Yamada, O. Iwata, K. Suzuki, S. Ohnuki, Y. Ohya, Y. Kato, T. Hasunuma, S. Matsusaka, M. Yamagishi, M. Yazawa, S. Uemura, K. Nagasawa, H. Watarai, D. Di Carlo, K. Goda*

*Corresponding author. Email: a_isozaki@chem.s.u-tokyo.ac.jp (A.I.); goda@chem.s.u-tokyo.ac.jp (K.G.)

The PDF file includes:

Supplementary Notes S1 and S2
Figs. S1 to S9
Table S1
Legends for movies S1 to S6

Other Supplementary Material for this manuscript includes the following:

(available at advances.sciencemag.org/cgi/content/full/6/22/eaba6712/DC1)

Data files S1 and S2
Movies S1 to S6

Supplementary Materials

Supplementary Note 1. Effect of the inter-droplet distance and electrode design on droplet sorting. The inter-droplet distance is a critical parameter of the SADA sorter. When the inter-droplet distance is too small, the non-target droplet either preceding or following a target droplet is also pulled upon actuation of the electrode array, thus resulting in a sorting error. To obtain a deeper understanding of the effect of the inter-droplet distance on the sorting performance, we performed computational simulations based on the simulation model shown in fig. S1 with some dimensional modifications. Specifically, we conducted the simulations based on the finite element method, varying the inter-droplet distance d, the width of the driving electrodes w, and the x-position of droplets x to obtain useful information for designing/replicating a SADA sorter. In these simulations, the diameter of droplets and the relative permittivity of the carrier oil is set to 64.5 μm (~140 pL in volume) and 2, respectively. Moreover, the first driving electrode is activated while the other electrodes are grounded. After performing these simulations, we found the ratio of the averaged dielectrophoretic force applied to a target droplet (F_t) to the averaged dielectrophoretic force applied to the non-target droplet preceding the target droplet (F_n):

$$R = \frac{\int_{-3w}^{-w} F_t dx}{\int_{-3w}^{-w} F_n dx}.$$

The location of the target droplet within the microchannel is aligned with the center of the first driving electrode (activated electrode) when $x = -2w$. The simulation results are summarized in figs. S7A and S7B. Fig. S7A indicates that the minimum inter-droplet distance necessary for obtaining a certain ratio increases as the width of the driving electrode increases. We assumed that the ratio must be more than 20 to effectively pull a single target droplet at a time without affecting other droplets and then developed fig. S7B to show the relation between the minimum inter-droplet distance and the width of the driving electrodes. The relation shown in fig. S7B indicates that the smaller the electrodes, the smaller the minimum inter-droplet distance, which leads to a higher sorting throughput. On the other hand, fig. S7B also shows that the dielectrophoretic force applied to a target droplet increases as the width of the driving electrodes increases, saturating at $w = $ ~100 μm. These results indicate that there is a trade-off relation between the minimum inter-droplet distance and the dielectrophoretic force applied to a target droplet as a function of the width of the driving electrodes. Based on these results, we designed the driving electrodes so that their widths are 100 μm. Note that further optimization of the electrode design may be necessary, depending on the droplet volume.

Supplementary Note 2. Effect of the physical properties of droplets on droplet breakage. Droplet breakage is caused by the multi-step structural deformation of droplets due to dielectrophoretic force and fluidic shear stress. The droplet deformation depends not only on the intensity and spatial distribution of the external force, but also on the physical properties of droplets. Specifically, the viscosity and mass of droplets cause droplets to deform while the interfacial stress between droplets and the surrounding medium resists the droplet deformation. In other words, the deformability of droplets increases with an increase of capillary number and Weber number, each of which is a dimensionless number defined by the ratio of viscosity to interfacial stress and the ratio of inertia to interfacial stress, respectively.
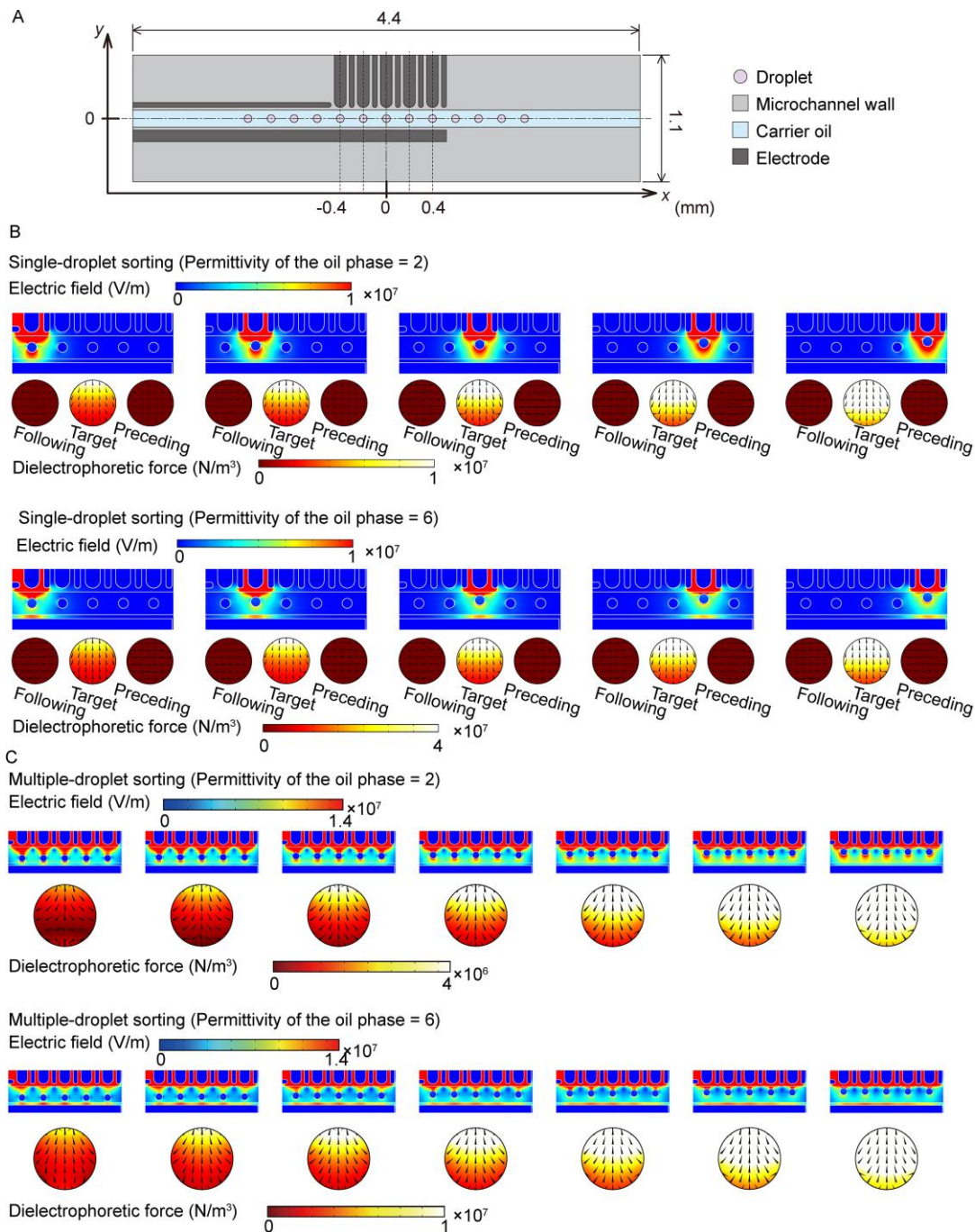
Fig. S1. Simulations of the SADA with grounded electrodes. (**A**) Simulation model. (**B**) Simulation of single-droplet sorting showing the electrical fields along the microchannel and the dielectrophoretic forces on the target droplet and the droplets preceding (right) and following (left) the target droplet. (**C**) Simulation of multiple-droplet sorting showing the electrical fields along the microchannel and the dielectrophoretic force on the droplet at x = 0 mm. In this simulation, we used water for the material of the droplets, which has an electrical conductivity of 5.5×10^{-6} S/m and a relative permittivity of 78; PDMS for material of the microfluidic channel walls, which has an electrical conductivity of 0 S/m and a relative permittivity of 2.75; Au for the material of the electrodes, which has an electrical conductivity of 45.6×10^6 S/m and a relative permittivity of 1.
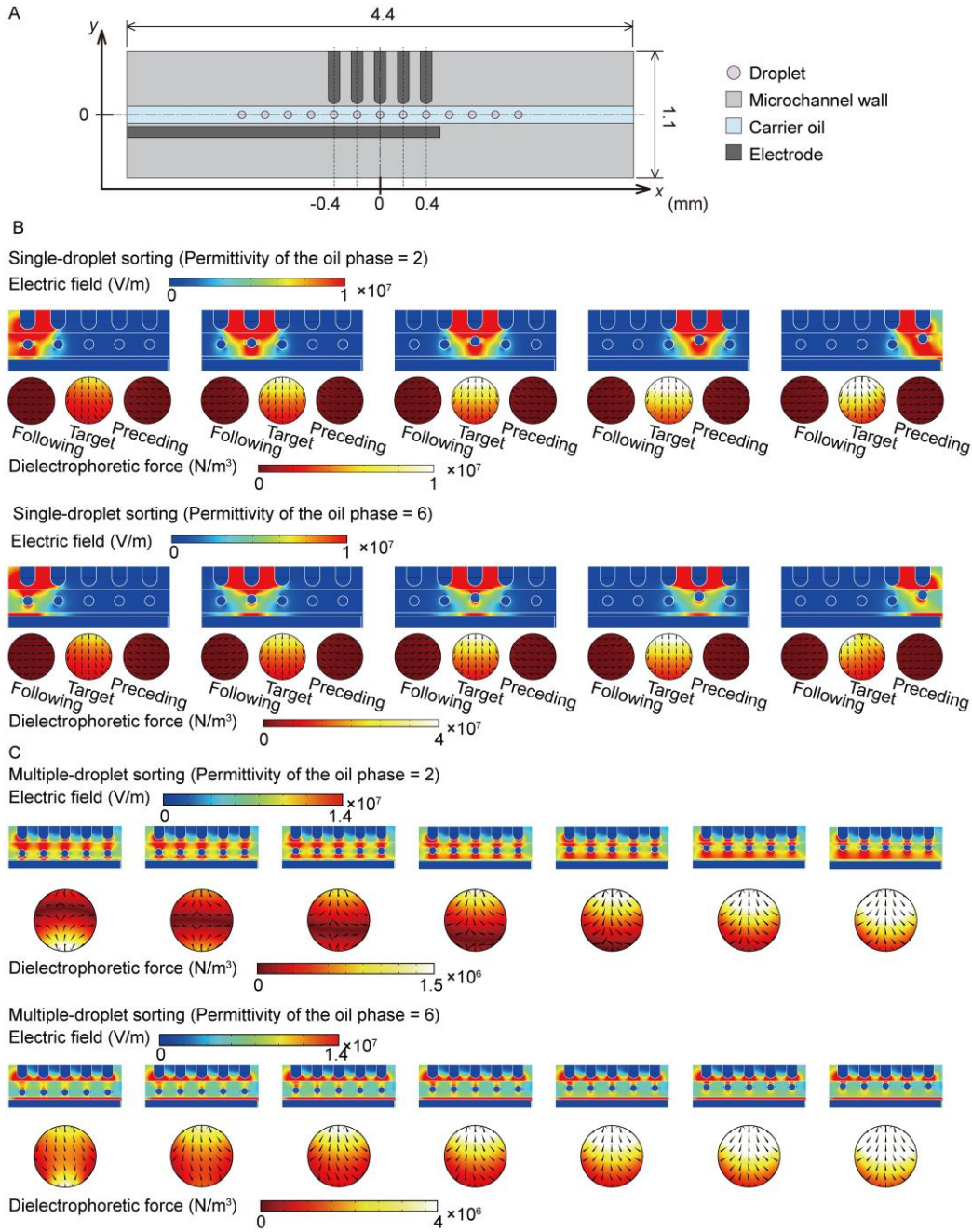
Fig. S2. Simulations of the SADA without grounded electrodes. (**A**) Simulation model. (**B**) Simulation of single-droplet sorting showing the electrical fields along the microchannel and the dielectrophoretic forces on the target droplet and the droplets preceding and following the target droplet. (**C**) Simulation of multiple-droplet sorting showing the electrical fields along the microchannel and the dielectrophoretic force on the droplet at $x = 0$ mm. In this simulation, we used water for the material of the droplets, which has an electrical conductivity of 5.5×10^{-6} S/m and a relative permittivity of 78; PDMS for material of the microfluidic channel walls, which has an electrical conductivity of 0 S/m and a relative permittivity of 2.75; Au for the material of the electrodes, which has an electrical conductivity of 45.6×10^{6} S/m and a relative permittivity of 1.
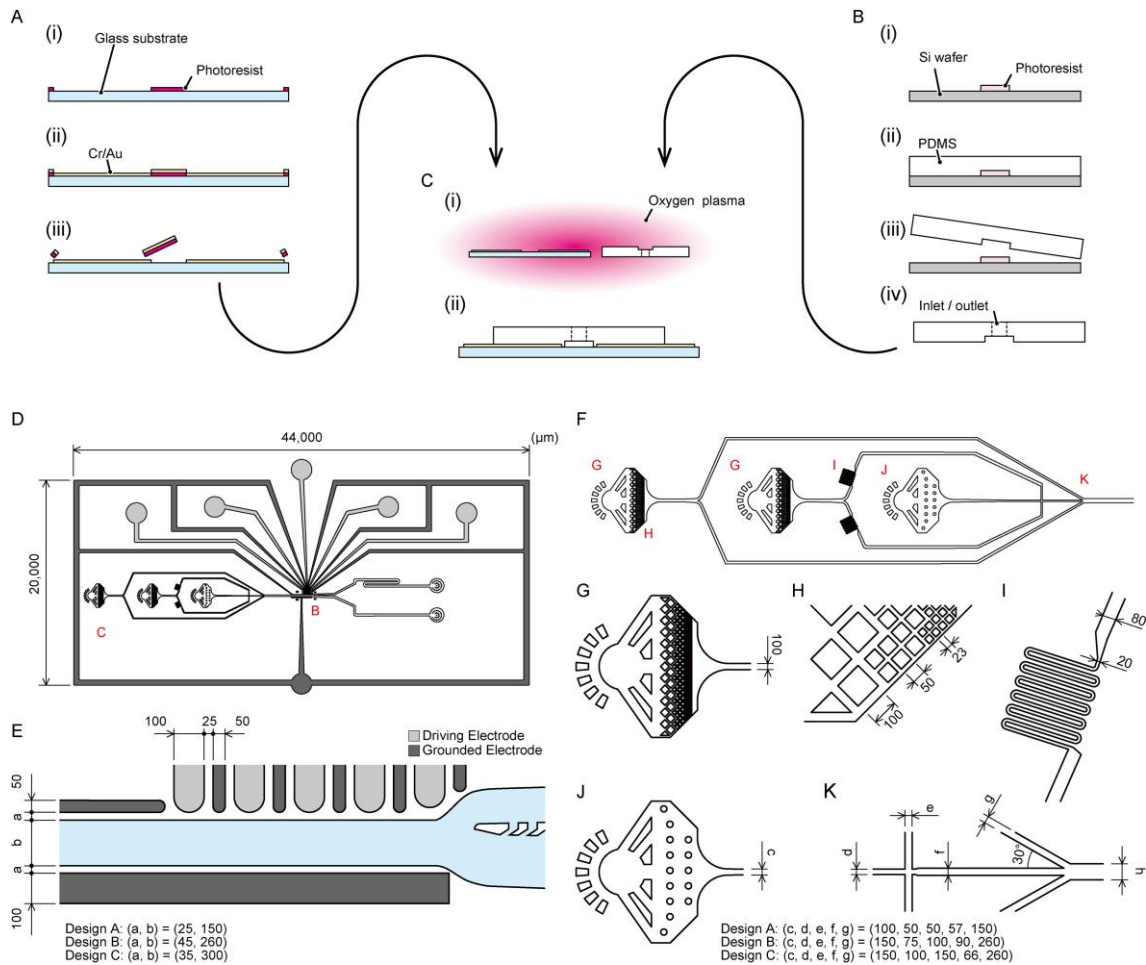
Fig. S3. Fabrication procedure and physical dimensions of the SADA chip. (**A**) Procedure for fabricating the electrodes using a lift-off process. (i) Photoresist was patterned onto a glass substrate. (ii) A 10-nm-thick Cr layer and a 70-nm-thick Au layer were deposited onto the substrate. (iii) Excess metal was removed by a lift-off process, revealing the electrodes. (**B**) Procedure for fabricating the microchannel using a conventional soft lithography process. (i) A photoresist master structure was patterned onto a Si wafer. (ii) Uncured PDMS solution was poured onto the master structure, degassed in a vacuum chamber, and baked to cure. (iii) The cured PDMS mold was peeled off from the master structure. (iv) Three inlets and two outlets were produced with a hole puncher. (**C**) Procedure for assembling the SADA sorter. (i) The PDMS slab and the glass substrate were exposed to oxygen plasma. (ii) The surfaces of the PDMS slab and the glass substrate exposed to oxygen plasma were bonded to create the closed channel. (**D**) Whole design of the microfluidic chip. (**E**) Enlarged view of the SADA. (**F**) Enlarged view of the inlets, droplet generator, and accelerator. (**G**) Enlarged view of the inlet for the oil phase. (**H**) Enlarged view of the filter for the oil phase. (**I**) Enlarged view of the hydrodynamic adjustor for dispersing the sample flow. (**J**) Enlarged view of the inlet for the sample phase. (**K**) Enlarged view of the droplet generator (cross-junction on the left) and accelerator (V-junction on the right). The designs A, B, and C are used for ~100-pL, ~500-pL, and ~1-nL droplet sorting, respectively.
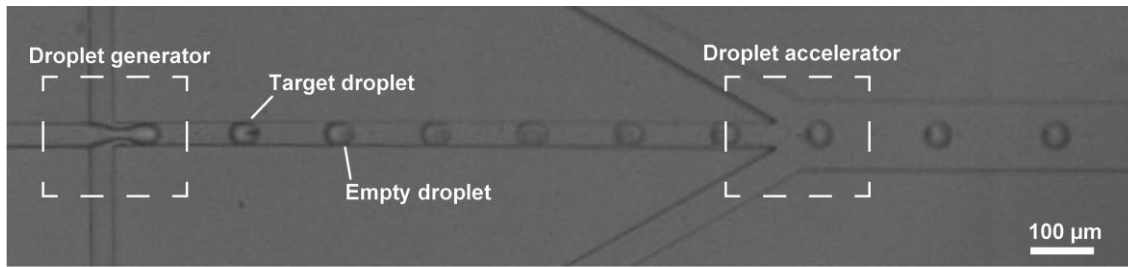
Fig. S4. Image of the droplet generator and the droplet accelerator. The size of the droplets generated in the image is 110-pL. *Euglena gracilis* cells were suspended in the dispersed phase and encapsulated in droplets. The flow rates of the dispersed phase, continuous phase, and spacing phase are 10, 30, and 125 µL/min, respectively.

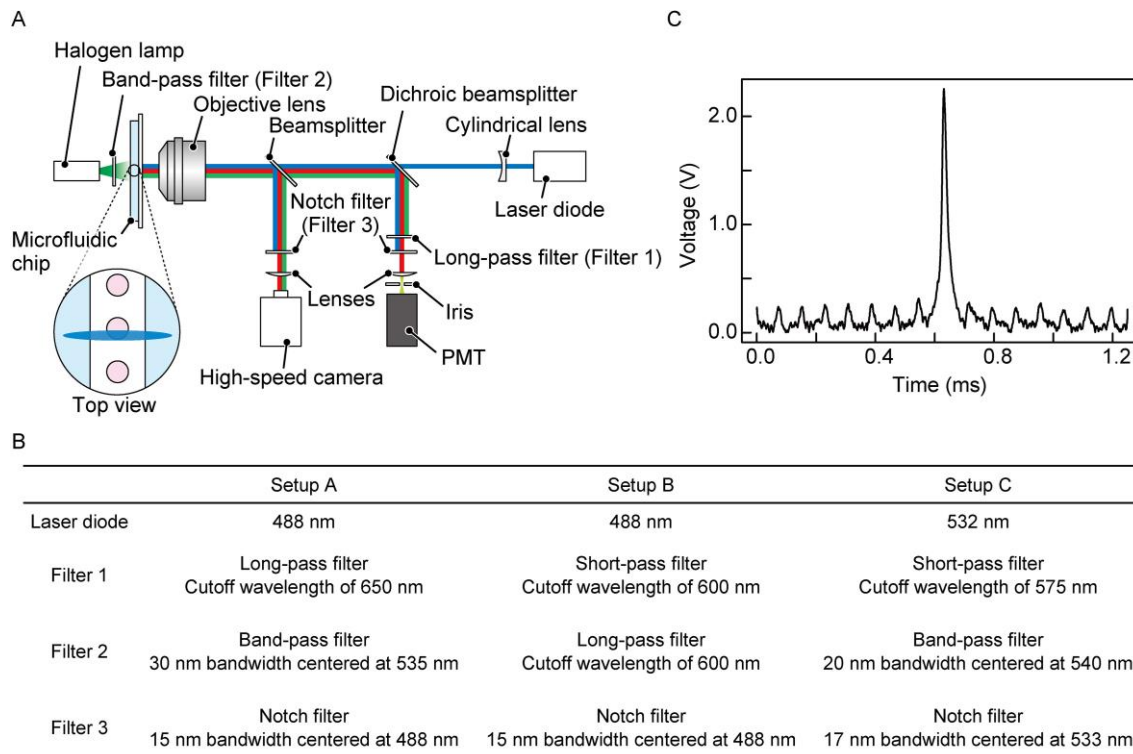|	Setup A	Setup B	Setup C
Laser diode	488 nm	488 nm	532 nm
Filter 1	Long-pass filter Cutoff wavelength of 650 nm	Short-pass filter Cutoff wavelength of 600 nm	Short-pass filter Cutoff wavelength of 575 nm
Filter 2	Band-pass filter 30 nm bandwidth centered at 535 nm	Long-pass filter Cutoff wavelength of 600 nm	Band-pass filter 20 nm bandwidth centered at 540 nm
Filter 3	Notch filter 15 nm bandwidth centered at 488 nm	Notch filter 15 nm bandwidth centered at 488 nm	Notch filter 17 nm bandwidth centered at 533 nm

Fig. S5. Optical detection and monitoring system. (**A**) Fluorescence/autofluorescence from the cell encapsulated in a droplet is excited by the laser that is cylindrically shaped and focused onto the microfluidic chip. The emitted fluorescence/autofluorescence is detected by the PMT. The droplet motion is monitored by the high-speed camera. (**B**) Components for the optical detection and monitoring system. (**C**) Typical PMT signal from a B5F6 hybridoma clone during sorting. Subtle fluorescence signals from empty droplets are evident because the dye solution slightly remains in the dispersed phase. The signal-to-noise ratio is approximately seven, which is sufficient to recognize the target droplets containing the clone.
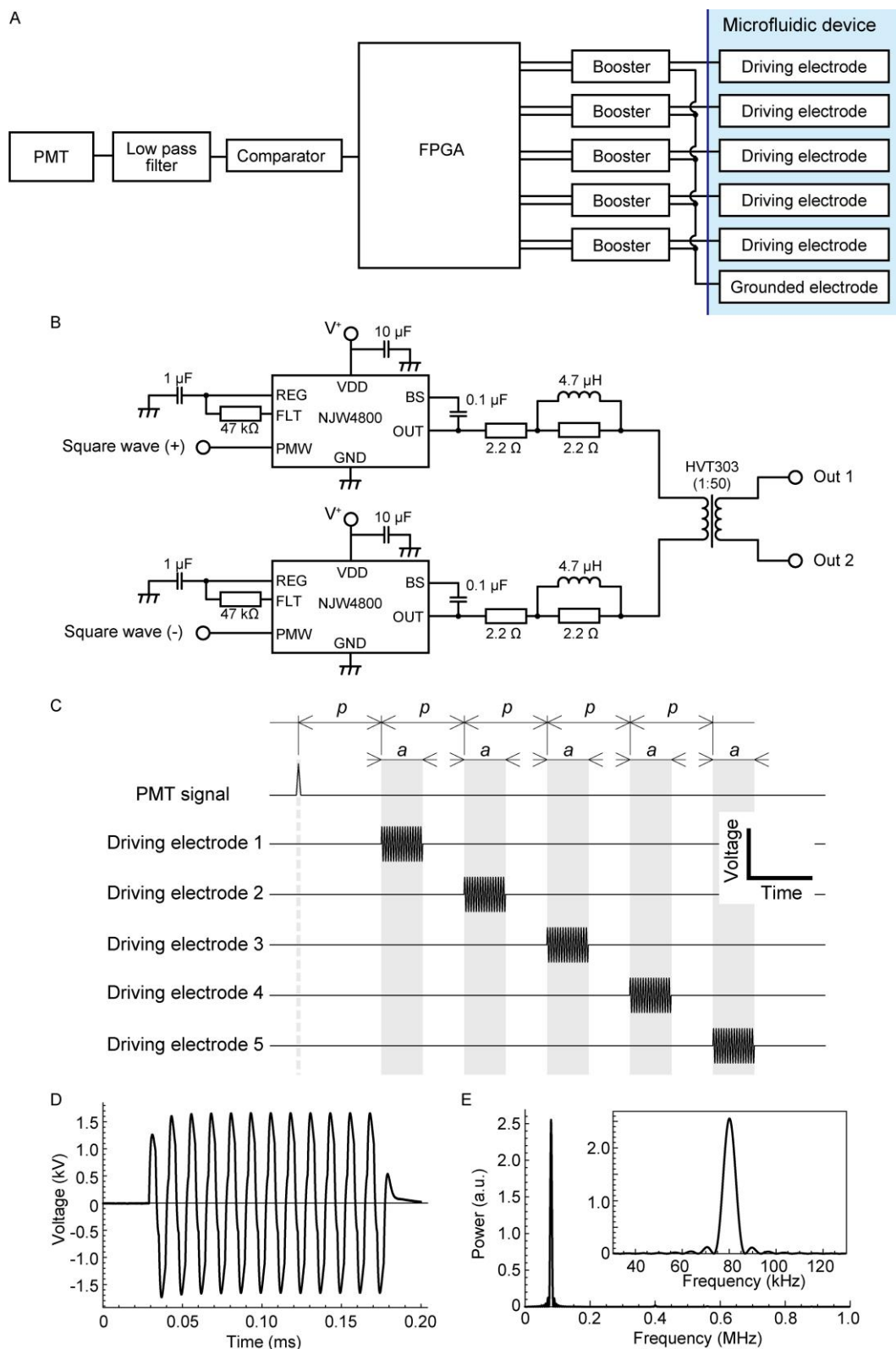
Fig. S6. Electronics for operating the SADA chip. (**A**) Block diagram of the electronics for controlling the SADA. The electrical signals from the PMT are sent to the FPGA board via the low-pass filter and the comparator. The FPGA sends control signals (square waves) to the booster circuits with a constant time delay that can be tuned according to the droplet flow speed. The boosted signals are applied to the driving electrodes and the grounded electrode. (**B**) Electric circuit of the boosters to generate ~2 kV$_{pp}$. The key constituents of the booster circuit are the two half-bridge drivers (New Japan Radio Co.,

Ltd., NJW4800) and a transformer (Nihon Pulse Industry Co, Ltd., HVT303). The half-bridge drivers receive and amplify the antiphase square waves that are generated by the FPGA board according to the input power (V^+ in the figure), which is typically 20 V. The amplified signals are combined and boosted by the transformer by a factor of ~60, which depends on the electric properties of the device connected to the output ports (Out 1 and Out 2 in the figure). (C) Conceptual diagram of the timings of the applied voltages onto the driving electrodes. Typically, the period to apply voltage p and application time a are shown in table S1. (D) Electric signal by the boosters in the time domain. The voltages applied to the half-bridge drivers are 28 V. (E) Electric signal by the boosters in the frequency domain. The peak frequency is approximately 80 kHz.
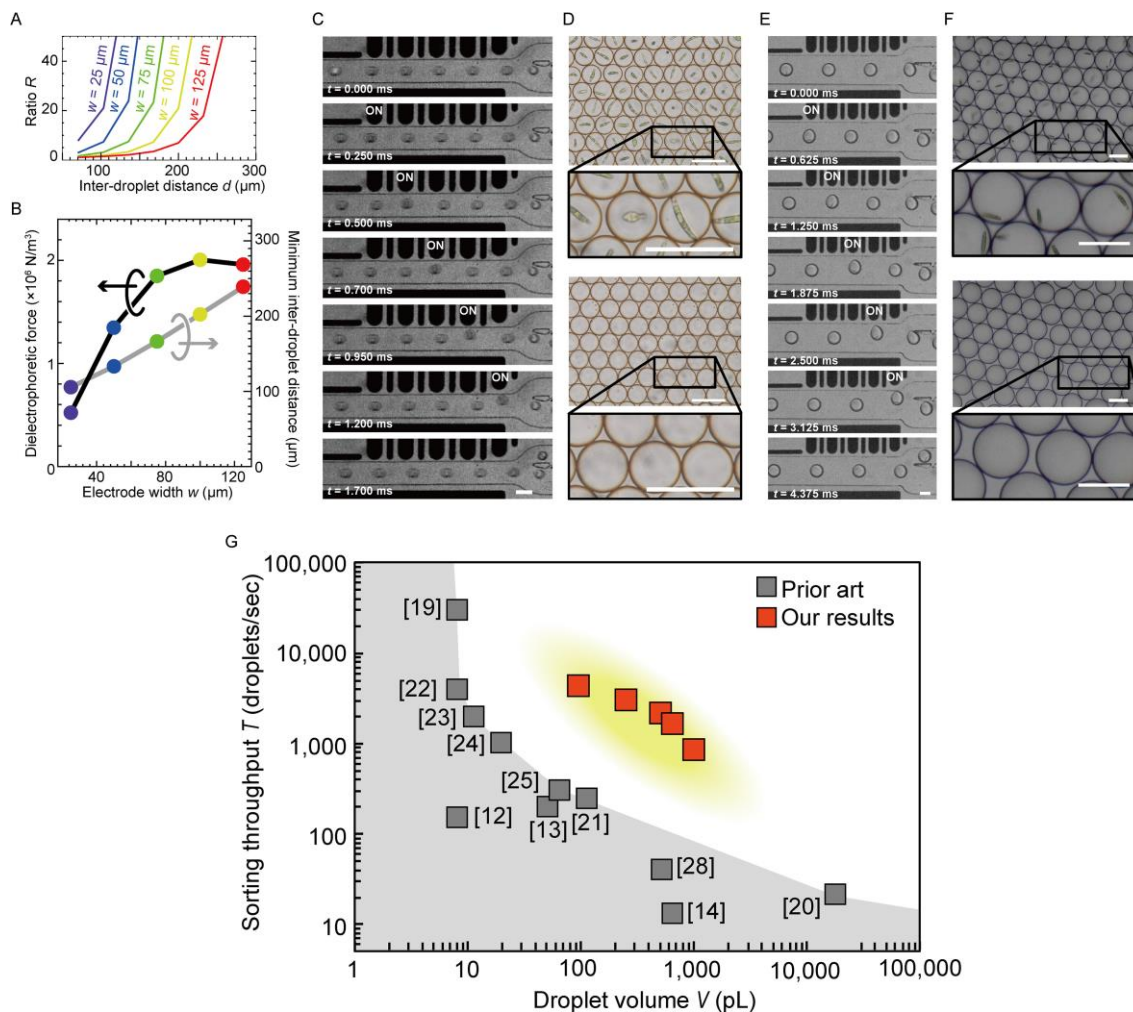

Fig. S7. Performance of the SADA sorter. (**A**) and (**B**) Computational simulations of dielectrophoretic force applied to droplets with varying parameters. The parameters varied are the inter-droplet distance d, the width of electrodes w, and the position of the droplets x. See Supplementary Note 1 for more details. (**C**) Demonstration of sorting a cell-encapsulating droplet (~95-pL in volume) with the SADA sorter. See movie S3 for a complete movie. (**D**) Bright-field images of SADA-sorted and -unsorted ~95-pL droplets with a high sort purity of 99.2%. (**E**) Demonstration of sorting a cell-encapsulating droplet (~1-nL in volume) with the SADA sorter. See movie S4 for a complete movie. (**F**) Bright-field images of SADA-sorted and -unsorted ~1-nL droplets with a high sort purity of >99.7%. Scale bars: 100 μm. (**G**) Complete version of the performance of the SADA sorter in comparison with the prior art.
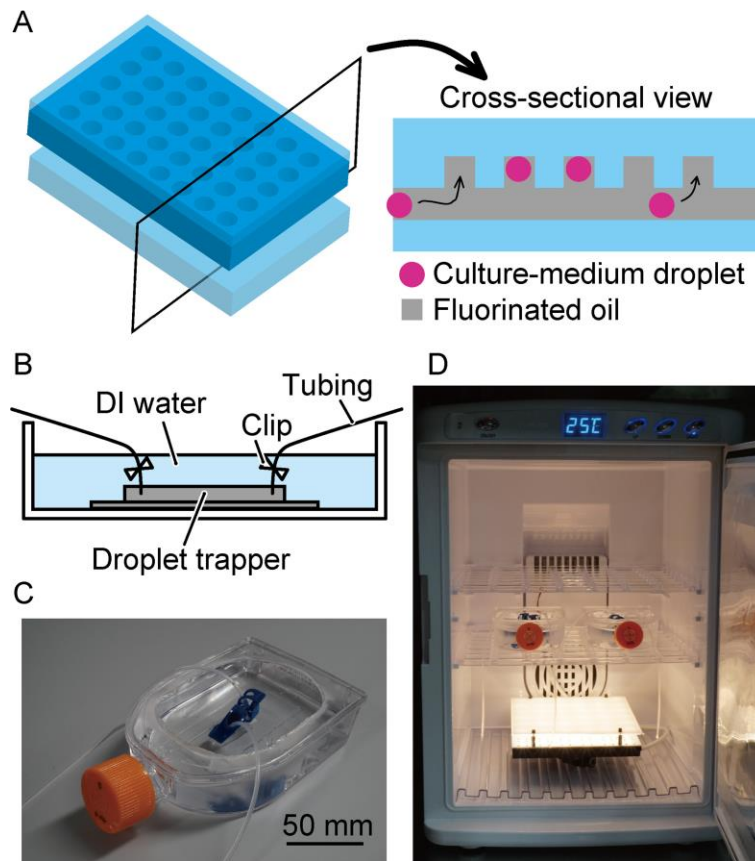
Fig. S8. Incubation and observation of *E. gracilis* cells encapsulated in droplets in a droplet trapper. (**A**) Schematic of the droplet trapper. The microwells in the droplet trapper trap and store the injected droplets because of the lower density of culture medium compared to the fluorinated oil. (**B**) Schematic and (**C**) picture of the droplet trapper submerged in deionized water in a flask. To prevent evaporation of droplets, droplet trappers are submerged in a flask filled with water. (**D**) Configuration of the custom-made growth chamber consisting of a temperature controller and a warm-white LED lighting with a 12h/12h light/dark cycle. Photo credit: Akihiro Isozaki, University of Tokyo.
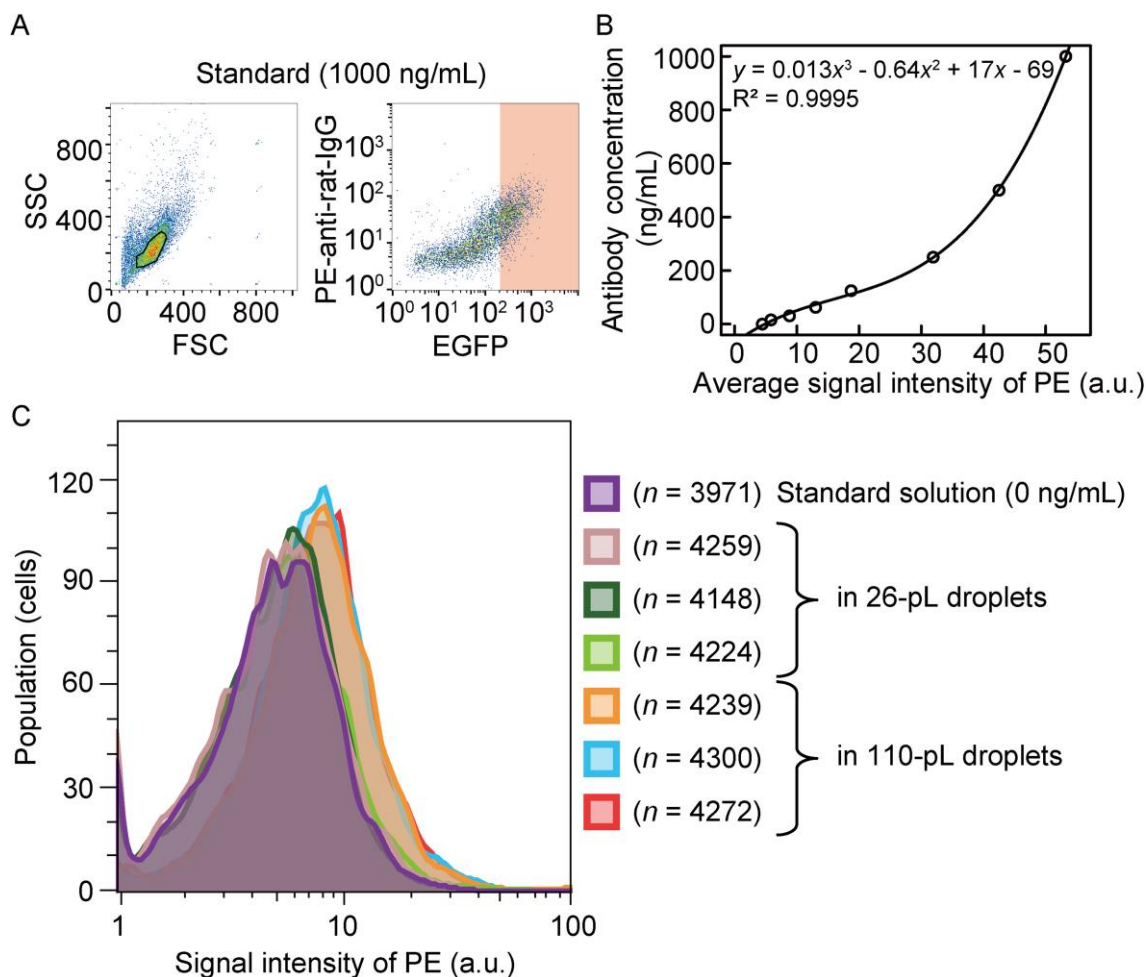
Fig. S9. Quantitative analysis of antibody production from hybridoma cells. (**A**) Example of the gating strategy. Live cells were gated by the scatter plots of FSC and SSC intensities (black-polygon region). Then, EGFP⁺ cells were gated (pink shadow region) and analyzed by signal intensities of PE. (**B**) Standard curve for quantitative analysis of antibody production of hybridoma cells in droplets. The standard curve was obtained using a cell analyzer (BD FACS Calibur). Standard solutions (i.e., mIL-17RB mAb) of known concentrations, ranging from 0 to 1000 ng/mL, were prepared and used to obtain the standard curve. (**C**) Histograms of signal intensities of PE. The signal intensities of the PE can be converted to the concentrations of antibody produced using the standard curve. The histograms confirm that the antibody production of hybridoma cells in large droplets (110 pL) is higher than those in small droplets (26 pL).

**Table S1. Typical parameters of the SADA operation.**

Droplet size (pL)	95	1000
Flow rate of dispersed phase (μL/min)	25	50
Flow rate of continuous phase (μL/min)	100	80
Flow rate of spacing phase (μL/min)	250	130
Flow speed of droplets (m/s)	0.9	0.35
Throughput of droplet generation (droplets/sec)	4,400	850
Applied voltage (kV_{pp}) to 1st electrode	1.51	25.0
Applied voltage (kV_{pp}) to 2nd electrode	1.45	24.5
Applied voltage (kV_{pp}) to 3rd electrode	1.36	24.0
Applied voltage (kV_{pp}) to 4th electrode	1.26	23.2
Applied voltage (kV_{pp}) to 5th electrode	1.30	23.2
Period of applied voltage (ms)	0.22	0.57
Application time (ms)	0.22	0.50
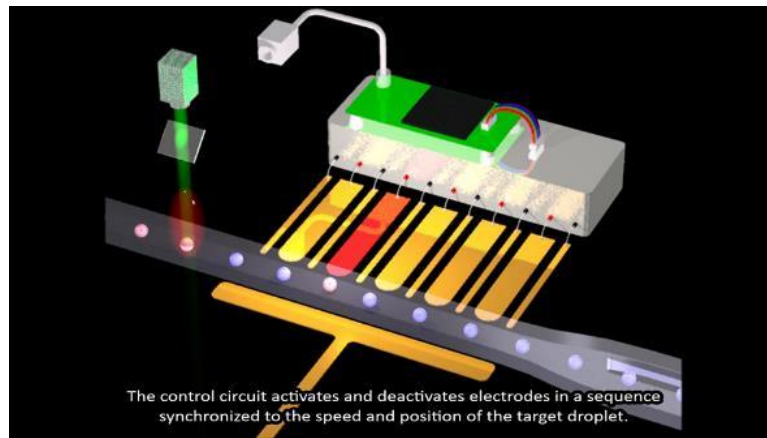
Movie S1. Animated movie that shows the functionality of the SADA.

5.277 ms
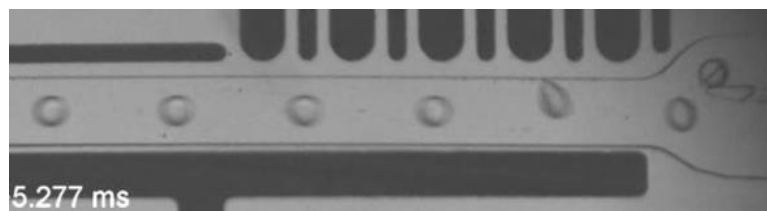
Movie S2. High-speed imaging of the sorting process of the SADA sorter (The volume of sorted droplets: 140 pL). Cell-encapsulating droplets (140 pL in volume) were sorted from a mixture of cell-encapsulating and numerous empty droplets at the throughput of 2,384 droplets/sec. The movie was recorded in a high-frame-rate mode (with low image quality).

10.050 ms
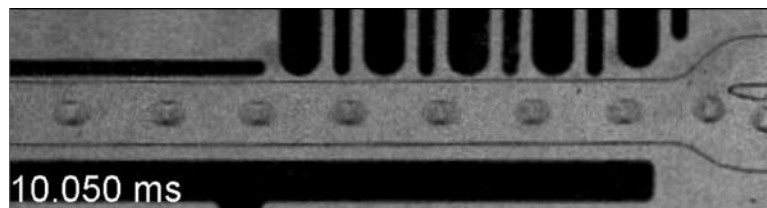
Movie S3. High-speed imaging of the sorting process of the SADA sorter (The volume of sorted droplets: 95 pL). Cell-encapsulating droplets (95 pL in volume) were sorted from a mixture of cell-encapsulating and numerous empty droplets at the throughput of 4,400 droplets/sec. The movie was recorded in a high-frame-rate mode (with low image quality).


0.000 ms

Movie S4. High-speed imaging of the sorting process of the SADA sorter (The volume of sorted droplets: 1 nL). Cell-encapsulating droplets (1 nL in volume) were sorted from a mixture of cell-encapsulating and numerous empty droplets at the

throughput of 850 droplets/sec. The movie was recorded in a high-frame-rate mode (with low image quality).

Movie S5. High-speed imaging of the sorting process of the SADA sorter using three replicated devices (The volume of sorted droplets: 1 nL). Cell-encapsulating droplets (1 nL in volume) were sorted from a mixture of cell-encapsulating droplets and numerous empty droplets. To validate the device-to-device reproducibility, three replicated sorters were fabricated and tested. The movie was recorded in a high-frame-rate mode (with low image quality).
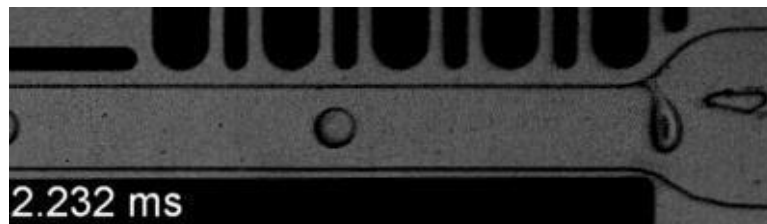
Movie S6. High-speed imaging of an unsuccessful sorting process (with a droplet of 140 pL in volume) using a single driving electrode of the SADA sorter. Cell-encapsulating droplets (140 pL in volume) were broken by applying high voltage of 2.6 kV_{pp} at the fifth electrode. The movie was recorded in a high-frame-rate mode (with low image quality).